quaternary

MDPI

Article

Selected Grain-Size and Geochemical Analyses of the Loess-Paleosol Sequence of Pécel (Northern Hungary): An Attempt to Determine Sediment Accumulation Conditions and the Source Area Location

László Makó [1,2,*], Dávid Molnár [1,2], Boglárka Runa [1], Gábor Bozsó [2,3], Péter Cseh [1,2], Balázs Nagy [1,2] and Pál Sümegi [1,2]

[1] Department of Geology and Paleontology, University of Szeged, H-6722 Szeged, Hungary; molnard@geo.u-szeged.hu (D.M.); runaboglarka@gmail.com (B.R.); cspeti94@gmail.com (P.C.); nagba88@gmail.com (B.N.); sumegi@geo.u-szeged.hu (P.S.)
[2] Long Environmental Changes Research Team, Interdisciplinary Excellence Centre, Institute of Geography and Earth Sciences, University of Szeged, H-6722 Szeged, Hungary; bozso.gabor@geo.u-szeged.hu
[3] Department of Mineralogy, Geochemistry and Petrology, University of Szeged, H-6722 Szeged, Hungary
* Correspondence: makol@geo.u-szeged.hu

Abstract: The loess-paleosol profile near the settlement of Pécel has a notable size among the loess-paleosol sequences of the Northern Carpathian territories. Therefore, comprehensive sedimentological examinations were performed to understand the profile and the information preserved in it. The past periodicity and intensity of winds were showed by particle composition studies (GSI, U-ratio). At least two source areas can be presumed based on geochemical indices (CIA, CIW, Rb/Sr, Zr/Rb). Based on the characteristics of the chemical composition of sulphide minerals (P, S, Pb, Ni, As sulphides), the lower 10 m of the profile was supposed to be transported from the NW direction (Buda Thermal Karst, Börzsöny, Cserhát). Sufficient information is not yet available in order to determine the source area of the upper 10 m. By using the mentioned indexes, major developing and weathering horizons also could be identified.

Keywords: geochemistry; loess; loess-paleosol sequence; Pécel; sedimentology; weathering; source area

Citation: Makó, L.; Molnár, D.; Runa, B.; Bozsó, G.; Cseh, P.; Nagy, B.; Sümegi, P. Selected Grain-Size and Geochemical Analyses of the Loess-Paleosol Sequence of Pécel (Northern Hungary): An Attempt to Determine Sediment Accumulation Conditions and the Source Area Location. *Quaternary* **2021**, *4*, 17. https://doi.org/10.3390/quat4020017

Academic Editor: Jef Vandenberghe

Received: 31 March 2021
Accepted: 21 May 2021
Published: 26 May 2021

1. Introduction

The complex investigation of loess-paleosol profiles aims at the detection of paleoclimatic and paleoecological changes of the Quaternary period [1–16]. The sedimentological (particle size composition) and geochemical analyses of loess-paleosol sequences can reveal environmental factors like the prevailing wind direction [17–19], wind intensity [20], precipitation intake [21] and weathering conditions and parameters [22,23]. The high-resolution sampling of the profiles supported by a sufficient amount of age data allows the examination with the resolution of decades and centuries. Our sediment samples cover a relatively short time interval because of the resolution of the sampling (4 cm), which provides the detection of so-called microcycles [14,15,24].

The graphical interpretation of grain size distribution could supplement the investigations with relevant information. One of these is the identification of loess and paleosol levels by the analysis of grain size fractions in the diagrams. Since loess predominantly comprises medium and coarse silt [20], a relatively high sand or clay content indicates a change in the accumulation conditions [20]. The high clay content could be the result of postgenetic processes, while an increased sand content suggests a change in the energy of the transport medium (in this case, rivers and wind) [20]. Weathering has a prominent role in the postgenetic processes, which causes an increase in the proportion of the fine fraction by the disintegration and fragmentation of larger sediment particles [20].

The loess-paleosol section of Pécel is situated in the western area of the Gödöllő Hills. These hills, with an area of 550 km^2, are rich in natural and landscape values. The elevation of the area ranges between 130 and 344, with a gradual decrease towards SE [25]. The dominant geomorphological forms are the two NW-SE lines of Valkói and Úri ridges (remnant ridges) and the Isaszegi Passage, a wind furrow, eroded by deflation [26]. On the surface of the ridges, loess-paleosol series up to the height of 40 m were developed, while Isaszaegi Passage area is covered by sand (sand dunes, sand sheets [26].

Since no previous research has been carried out on the loess-paleosol profile of Pécel, the authors aim to reconstruct the sedimentological conditions, processes during and following the deposition, and assume the degree of the weathering by the preliminary particle composition and geochemical investigations. This section can be a new area available for further paleoenvironmental and paleoclimatic research. Quaternary studies in Hungary can be supplemented with additional information with the 20–30-m-high profile of Pécel. It has a unique location in contrast to the loess-paleosol profiles of lowland (e.g., [12,14,15,27–29]) and foothill (e.g., [11,19,30,31]) regions of Hungary. Because of it, the North Hungarian Mountains and Buda Hills could play a role in the origin of the sediment of the Pécel profile.

A further aim of the research primarily could be the malacological examinations [32–35] or the radiocarbon/OSL dating of the profile. Moreover, age-depth models [15,27,36,37] can be constructed, accumulation rate can be calculated [17,18,37], and paleoenvironmental reconstruction can be carried out [11,12,27,31,35] by using these additional pieces of information. Furthermore, our data can be correlated with other profiles [8,38,39].

2. Materials and Methods

The loess-paleosol profile of Pécel (47°29′47″ N and 19°21′12″ E (Figure 1)) was sampled in 2019. The section with a height of approximately 18.72 m was created by using nine continuous sub-sections. All sub-sections were sampled with a resolution of 4 cm (468 samples). The preliminary particle composition and geochemical analyses were carried out at the University of Szeged.

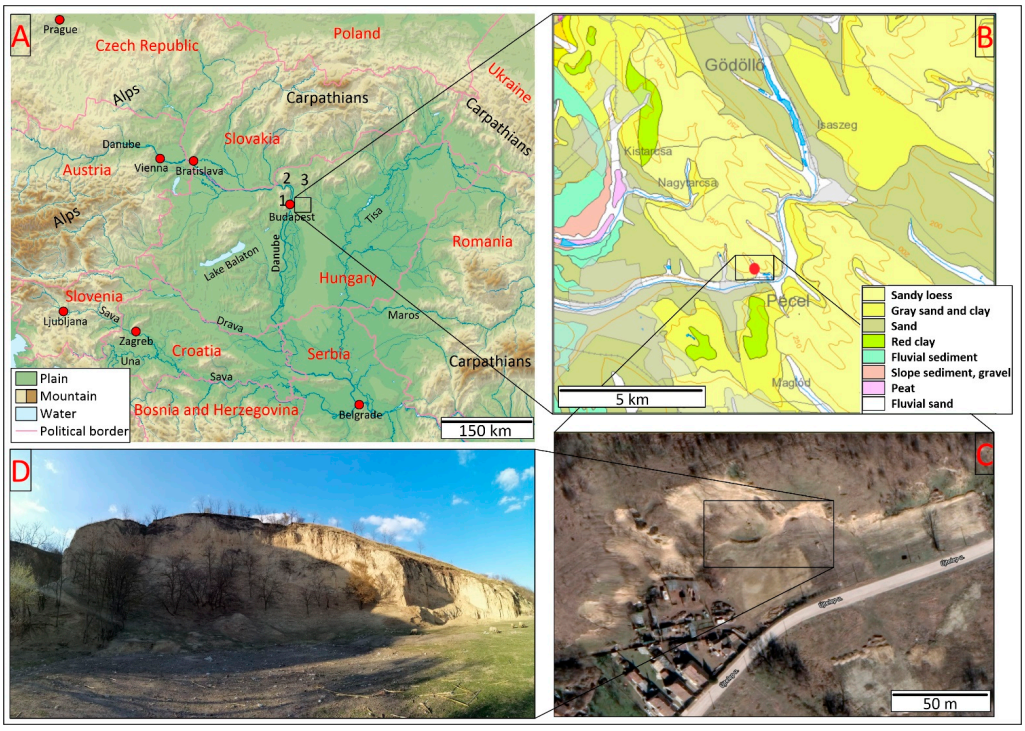

Figure 1. Location of the loess-paleosol sequence of Pécel in the Carpathian Basin ((**A**) figure: 1. Buda Thermal Karst, 2. Börzsöny, 3. Cserhát [40], (**B**) figure: surface formations [41], (**C**) figure: orthophotomap [42], (**D**) figure: selfmade site photo).

2.1. Grain Size Analysis

The determination of grain size composition was based on Bokhorst et al. [43]. Air dried samples were pre-treated in hydrogen peroxide (30% H_2O_2) and hydrochloric acid (10% HCl) bath to remove organic materials and carbonate from the sediment. Then, 30 mL of Calgon ($Na_2P_6O_{18}$) solution was added to 0.7 g of the sample to separate the individual granules. Immediately before the measurement, the samples were treated in an ultrasonic cleaner for 20 min to prevent the adhesion of the particles. The grain size composition was carried out with an Easysizer 20 laser sedigraph at the Department of Geology and Paleontology, University of Szeged. The source used is a 2 MW of energy, 0.6328 µm wavelength He-Ne laser [14]. The laser sedigraph measured 42 particle size ranges between 0.0001 and 0.5 mm using 54 built-in detectors based on the Mie scattering theory. Frequency and cumulative values were calculated by using the measured values. The results were arranged into particle size ranges based on the Wentworth scale [44] and plotted on separated line diagrams.

2.2. Grain Size Indices

The U-ratio and GSI values were calculated based on the particle composition results to determine the energy of the transport medium [45–47]. The U-ratio gives the ratio of coarse silt with medium and fine silt $\frac{16-44\ \mu m}{5.5-16\ \mu m}$. It can be used to distinguish glacial periods with significant aeolian transport (high U-ratio) and high wind speed and warm, wet interglacial periods of weak winds (low U-ratio). This is based on the observation that the predominant particle size of aeolian sedimentation in warmer interglacial periods is <16 µm, while in cold glacial periods it is >16 µm [46,48]. Clay (<5.5 µm) and fractions <44 µm are not taken into account in the calculation of U-ratio. Thus, information cannot be obtained about clay minerals that formed during secondary, postgenetic processes, as well as fine sand transported by saltation [46,49]. The "Grain Size Index" (GSI), introduced by Rousseau et al. [21], is quite similar to the U-ratio. The most significant difference between them is that clay fraction is also taken into account in the calculation of GSI $\frac{20-50\ \mu m}{<20\ \mu m}$. GSI values make possible the estimation of sedimentation, sediment transport and accumulation, which are closely related to the changes in wind speed [50]. High GSI values indicate increased frequency and intensity of wind storms in parallel with a higher sedimentation rate [18,50].

2.3. Geochemical Analysis

Samples (44) were chosen representatively and measured with a XRF instrument at the Department of Mineralogy, Geochemistry and Petrology, University of Szeged. After the homogenization of the selected samples, pellets were formed from 4 g of a sample with the addition of 1.5 g of Cereox adhesive under a pressure of 20 tons. For the evaluation of the measurement results, the data must be corrected with the 1100 °C "loss on ignition" (LOI—[51]) results of the samples. The following parameters were used: 50 kV excitation voltage, 40 mA anode current, palladium X-ray tube, LiF, PET monochromators, proportional and scintillation detectors, EZ Scan mode, 1200 s measurement time, semi-qualitative analysis in a vacuum. The cooling of the system was allowed by an argon/methane gas mixture.

2.4. Geochemical Indices

The examined major and trace elements are presented in percentage and ppm (mg/kg) respectively. Several geochemical indices were used to get information about the weathering conditions of the profile. Most of these are based on the mobility and exchangeability of water-soluble elements (e.g., [30,52–64]), which are caused by the ionic potential of alkali metals and alkaline earth metals [65,66]. Ca, Mg, and Sr are common alkaline earth metals in silicate minerals that are susceptible to weathering [52,64].

The indices used are the following: chemical index of alteration (CIA—[53]), chemical index of weathering (CIW—[67]), Rb/Sr ratio [56], Zr/Rb ratio [68,69]. The two major

element indices (CIA and CIW) are widespread weather indices in the fields of loess investigations, paleoclimatical, and paleoenvironmental reconstructions [30,52,53,58,61,62,64]. The Zr/Rb ratio has become important because of the extremely high Zr content, which is an excellent indicator of weathering horizons because of its high ionic potential as an insoluble, immobile element [64,66].

3. Results

The stratigraphic units and their boundaries were identified during the field sampling, while the lithostratigraphic description and separation were already performed in the laboratory. It includes the determination of the wet and dry color of each sample based on the Munsell color scale. The notations of Chinese loess sections [2,70–73] were used for the description of the lithological horizons.

3.1. Grain Size Composition

A well-developed paleosol complex (S3) can be identified between 1784 and 1872 cm (Figure 2), which can be divided into two parts. The proportion of the coarser particle size is constantly increasing with the decreasing of the finer ones. The predominant grain size fractions are medium and coarse silt with a high clay content of around 20%.

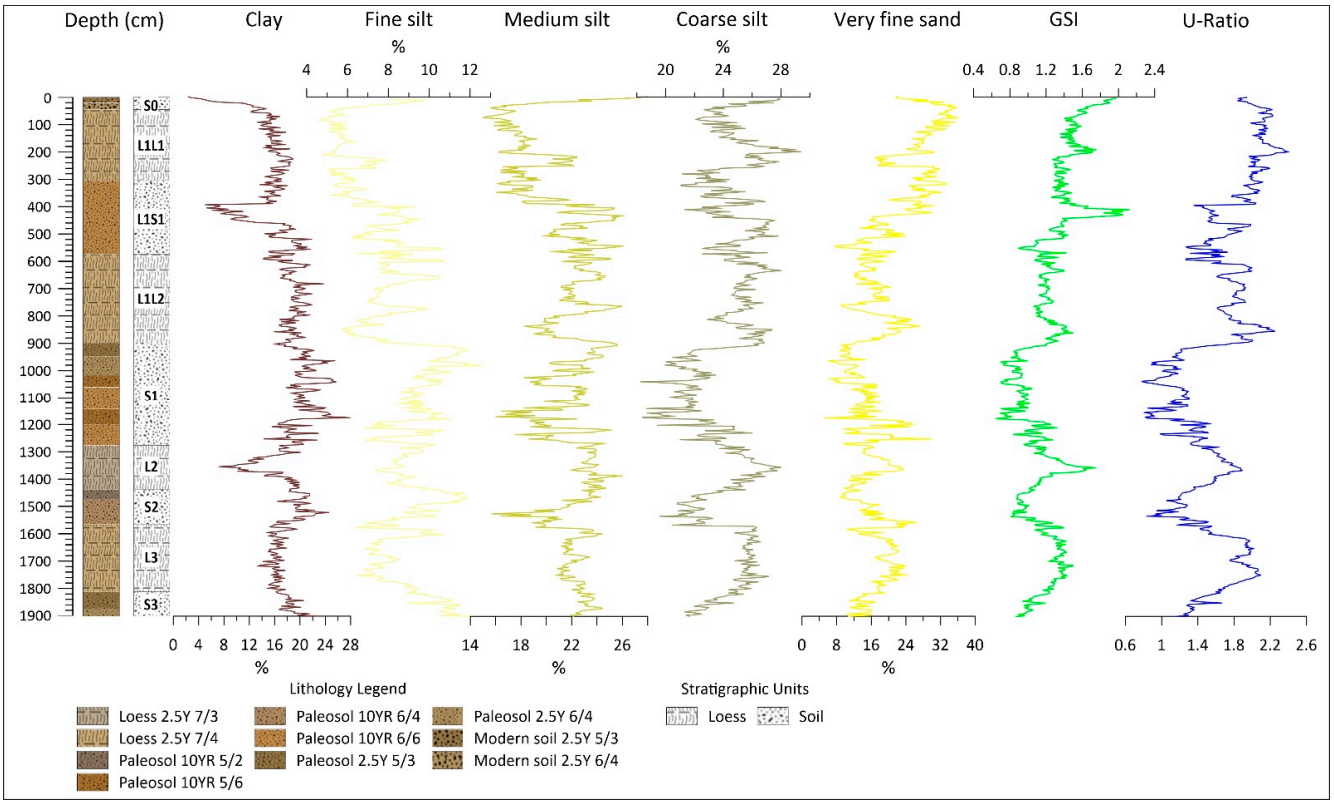

Figure 2. Grain size compositions plotted on separated line diagrams, GSI and U-ratio line diagrams [12,14,15,19,22,26–29].

A homogeneous loess layer (L3) can be observed between 1540 and 1784 cm with no change in its color. The change in particle size continues from the finer to the coarser fractions, thus coarse silt and very fine sand become predominant. A slight change was detected between 1680–1700 cm, where the proportion of fine and medium silt increases in contrast with the decreasing proportion of very fine sand.

Above the loess layer, between 1416 and 1540 cm, another paleosol layer lies (S2), which was divided into two parts, a lighter part between 1452–1540 cm and a darker bet-ween 1416–1452 cm. In the transition zone of the lower part and the L3 loess layer, the amount of very fine sand increases (26%), then decreases upwards. The clay content

declines on the boundary of the lower and upper part (1540 cm) with a slight increase in the proportion of coarse silt and very fine sand.

A well-developed homogeneous loess layer (L2) can be found above S2, between 1256 and 1416 cm, with carbonate concretions between 1350 and 1408 cm. The low proportion of very fine sand (10%) in the S2/L2 transition zone reaches its maximum at 1344 cm with almost 24%. From that point, it decreases back to 10% to the L2/S1 transition. It predominantly comprises coarse (24–28%) and medium (22–26%) silt. The clay content is the opposite of the sand content, shows its minimum (7%) at the maximum of the sand proportion. By the L2/S1 transition, its proportion gradually increases to 20%.

A diverse paleosol layer (S1) can be found between 884 and 1256 cm above the L2 loess layer, which can be divided into 6 parts based on its color. The first part, between 1180 and 1256 cm, is a light-colored section with a rhythmically changing proportion of very fine sand content between 1236 and 1256 cm (increasing from 9 to 30%, then decreasing to 10% again (1216 cm)). In 1200 cm, a minimum can be observed again, then to 1180 cm it increasing to 26%. The clay and very fine silt fraction follow the same trend with an inverse relation. Since outstanding values cannot be observed in geochemical indices, the reasons for this can be the changes of the source area, or the changes in the wind direction, or the drastic relapses in the energy of the transport medium several times. Such a notable trend cannot be observed in the cases of the other fractions. Above, between 1124–1180 cm, a darker part can be found, in which the latter trend continues up to 1160 cm. The proportion of the very fine sand decreases to 5%, while the proportion of clay and very fine silt fractions increase to 28% and 17%. The different grain size fractions in the next part of the paleosol level are characterized by only a few percent of oscillation. Between 1044–1124 cm, the clay, and medium and coarse silt become dominant, but the difference between the minimum and maximum values of each fraction is less than 5%. Between 1000–1044 cm, the trend of the lower parts reappears. The proportion of very fine sand decreases from 17 to 6% (1016 cm) and unlike before, the proportions of fine, medium and coarse silt increase. The presence of a weathering horizon was assumed here, which is also supported by the geochemical indices. Between 932 and 1000 cm, the proportion of fine sand is low, varying between 6–15%. The clay content is between 19–26%, the fine and medium sand are between 20–25% and 20–23%. The uppermost part of the S1 paleosol level can be found at 884–932 cm. The clay content decreases continuously up to a minimum of 16%, the average proportion of medium and coarse silt is 24–24%, with 9–12% of very fine sand. Carbonate concretions can be identified at 1248 cm and between 1188 and 1176 cm.

The next layer between 884–1044 cm consists of two loess layer with a buried paleosol between them. The lower loess layer (L1L2) is between 568–884 cm. The grain composition is gradually fining upwards. A significant change can be observed at 752 cm, where the proportion of fine silt increases, while coarse silt and very fine sand decreases and the clay content stagnates. The refining tendency of the sediment continues upwards. The abovementioned pattern reappears at 652 cm except for the slighter decrease in fine sand and clay content.

The intervening paleosol (L1S1) can be found between 300–564 cm. This part continues to roughen upwards in terms of grain size distribution. A change can be seen between 392 and 456 cm, where the average clay content of 16–20% decreases to 5% as well as coarse silt, meanwhile, all the other fractions increase significantly. The proportion of very fine sand also increases further to the L1S1-L1L1 boundary.

The same color as the L1L2 layer characterizes the uppermost part of the loess body (L1L1) between 44 and 300 cm. The very fine sand fraction in the layer is around 30% but decreases to 20% for 40 cm. Its proportion is constantly increasing from 216 cm and reaches a maximum of 36% at 80 cm. The opposite trend can be observed in the changes of the clay fraction. The proportion of very fine and fine silt ranges between 5–8%. Considering the averages, the very fine sand content becomes predominant with its 28% with 25% coarse silt and 18% medium silt proportions.

The top of the profile is the S0 recent soil layer, which was divided into two parts, a lower (20–44 cm) and an upper (0–20 cm). The clay fraction in the lower part is continuously decreasing from 14% to 6%, and the fine silt fraction increases by 1–2%. The average of the very fine sand proportion is 32%. The dominance of medium and coarse silt (24–28%) and the practically complete absence of clay fraction (2–6%) characterize the upper section. Besides, the proportion of very fine sand drops to 22% from 29%.

3.2. GSI/U-Ratio

GSI values (Figure 2) increase from 0.87 to 1.14 between 1600–1872 cm, and fall back to 0.9 between 1436–1448 cm. From this point, it rises and reaches 1.75 at 1336 cm. The lowest value of the entire profile is at 1156 cm with 0.69 and remains below 1 up to 904 cm. Below 60 cm, GSI values rise to 1.5, then decrease back below 1 for the next 90 cm. Up to 544 cm, it ranges between 0.9 and 1.4. A significant peak with the highest value (2.12) of the profile can be observed between 364–508 cm. Another peak (1.7) appears at 192–200 cm. Then it continuously decreases to 1.4 at 76 cm, from where it starts to rises again and reaches a value of 1.97 on the surface. The larger fluctuations in U-ratio can be explained with the consideration of the clay content in the calculation [45–47]. The movement of the trendlines is uniform, although the L3 layer (1540–1784 cm) indicates a positive protrusion. The most conspicuous ones are between 364–509 cm and 0–75 cm where the values differ from the trend. These anomalies can be explained by the extreme decrease of the clay fraction.

3.3. Geochemical Analysis

It can be concluded for the lithological change of S3 level (Figure 3), that Mg content gradually ceases and Mn content is quadrupled. The same pattern can be observed in the case of trace elements as Zr, Sr, Rb, Ni. A significant increase is detected in the values of As (from 0 ppm to 48 ppm) at the S3/L3 boundary. In L3, the amount of Ca gradually increase, while Mg, P, S elements show high variability. Pb, Cu and As significantly increase, but the other trace elements show a decreasing trend overall.

Several changes can be observed in the L2/S2 boundary. The amount of Ca and S halved while Mg increases to 6% from 0. Zr, Pb, Rb and Ni values also increase. Pb reaches its maximum (255 ppm).

S2 can be divided into two lithological layers. At their boundary, the major elements like Fe, Ca, Mg and S and trace elements like Sr, Pb, Cu increase, moreover Rb gradually increases up to S2/L2 boundary, where Na content also rises from 0 to 7%.

The highest p values of the profile were detected (0.5–0.6%) in the L2 loess body and the S1 paleosol layer above where Zr, Pb, Ni values decrease, and in the middle of the loess body Sr, Cu, Rb increase. S1 is divided into six lithological parts, however, it cannot be detected based on the geochemical results. The Fe content gradually decreases up to 1000 cm and reaches a maximum of 27% in the S1/L1L2 boundary zone. Mg, P, S, Zn, Pb, Ni, As is detected with a significant amount up to this zone, from this point Ca, K, Na and Zr elements become predominant. This general change is not significant in the case of Si, except for the decrease from 16% to 4% and the peaks (to 32%) in the upper part of the L1L1 and S0.

Significant changes cannot be seen in the L1L2 loess body except for the smaller peaks of Na, Sr and Ni. The highest Zr content (1781 ppm) is detected in the L1L2/L1S1 boundary. Fe and Ca decrease, while Si and K increase and a slight increase can be observed in Zr and Cu trace elements in the lower part of the L1S1 paleosol (492–496 cm). Rb content continuously increases from 73 to 106 ppm up to the boundary of L1L1, and a peak of Ti is detected (increases from 1–2 ppm to 7.5 ppm).

In the L1L1 loess body, Si, Mg and Al start continuously increase and Fe, Ca, Na (with a maximum of 9.3%) and Mn-and all trace elements- decrease from 172–176 cm. The Al content reaches its maximum at this level: between 0–56 cm ranges between 4.5–5.3%.

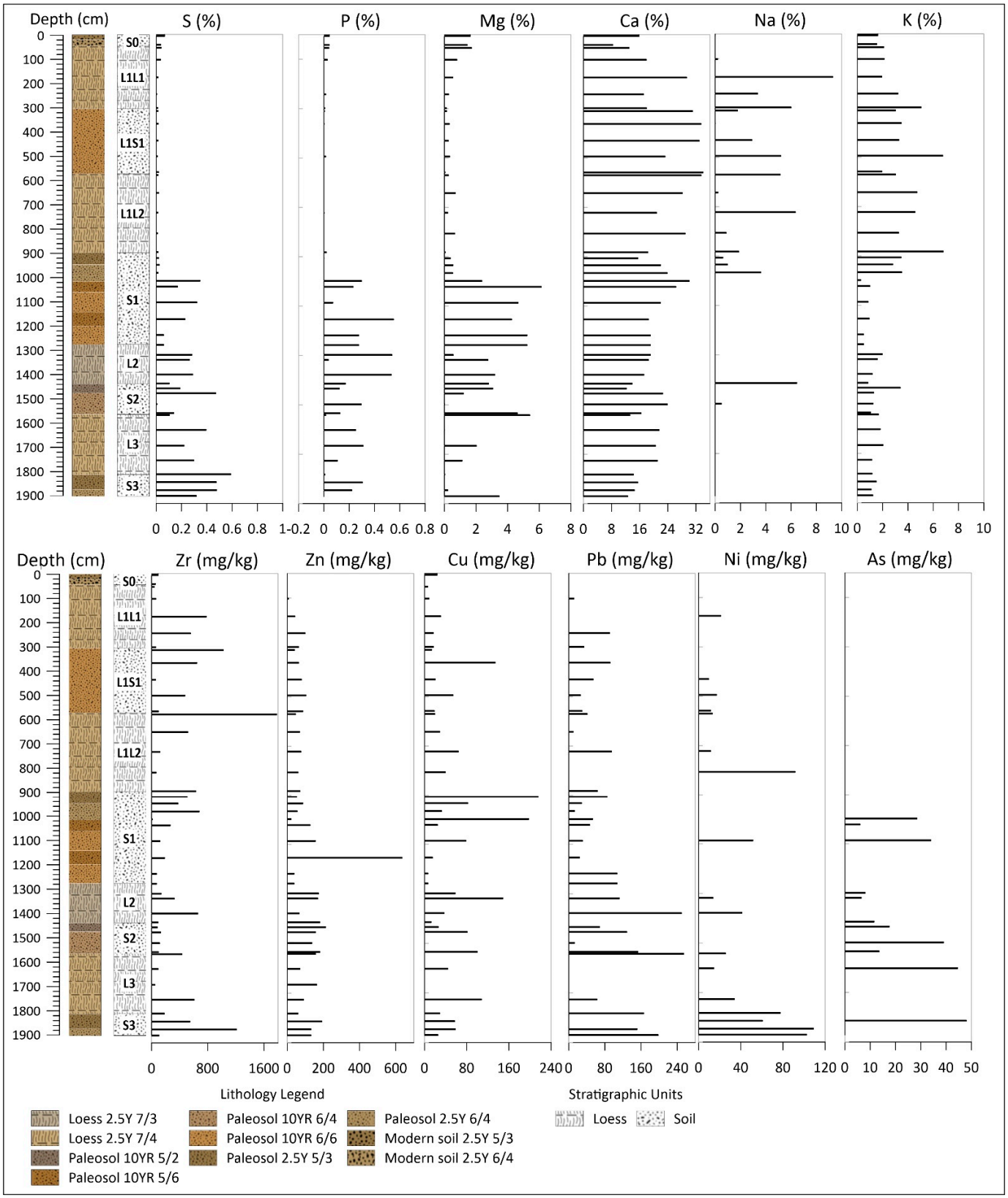

Figure 3. Highlighted geochemical results from XRF (major elements above, trace elements below).

3.4. Geochemical Indices

The examined geochemical indices suggest a weathering horizon if CIA [47], CIW [67] indices and Zr/Rb ratio [68,69] increase while Rb/Sr ratio [55] decreases. These character-

istics are caused by the high mobility of Rb, and moderate mobility of Sr and immobility of Zr element [55,64,68,69].

Nine major parts were distinguished within the profile based on the selected geochemical indices. The first layer is between 1780–1862 cm, where a peak of Zr/Rb (1844–1848 cm) and Rb/Sr (1812–1816 cm) can be found. The next level is between 1496–1604 cm, characterized by the positive shift of all examined indices. Above, between 1376–1456 Rb/Sr ratio is doubled, while a slight decrease of Zr/Rb and smaller fluctuation of CIA and CIW indices can be seen. The next level is between 1256–1320 cm, is characterized by a significant Rb/Sr ratio (2–3x value), a minor decrease of Zr/Rb and unchanged CIA, CIW ratios. It is followed by a larger part (804–1088 cm) with varying values of the different indices. The first major change appears between 1020–1024 cm, where the Rb/Sr ratio decreases and Zr/Rb increases. Then, up 932–936 cm, Rb/Sr ratio more than quadruples (0.89), Zr/Rb ratio decreases to nearly 0 (996–1000 cm) and then ranges between 3–6. CIA, CIW indices slightly drop at 964–968 cm, then increase to 904–908 cm and decrease again, which persists until the next part (556–644 cm). The highest protrusion of the Zr/Rb ratio in the entire profile (19) can be found here caused by the Zr value of 1781 ppm. Between 296–496 cm, CIA and CIW values do not show significant change except for a slight increase. In contrast, high Rb/Sr is associated with a low Zr/Rb ratio at 428–432 cm. In this and the next part, the latter two ratios show the opposite. The Zr/Rb ratio increases because of the presence of over 1000 ppm Zr and the Rb/Sr decreases.

Both CIA and CW indices decrease sharply in the penultimate part between 100–344 cm. Both indices reach their minimum value of 40 and 47, respectively. The Rb/Sr ratio also has a negative peak here, while Zr/Rb ratio increases.

The uppermost part can be observed from 56 cm to the surface (0 cm). At the boundary of L1L1/S0, the CIA and CIW indices reach their maximum within the entire profile (50 and 60, respectively), while the two other indices are at their minimum (0). Following this point, the CIA and CIW slightly decrease, Rb/Sr and Zr/Rb increase from zero to 0.3 and 12, respectively.

A weathering horizon occurs (Figure 4) between 1844–1848 cm within the S3 paleosol layer, which is characterized by high Zr content of 1209 ppm (Figure 3). The next weathering horizon is at the transition of L3-S2, where the Rb/Sr ratio moves in a positive direction. Its explanation can be the higher Rb content (115 ppm). The next weathered zone occurs in the upper part of the S2 paleosol. Rb/Sr and Zr/Rb ratios have an opposite trend than the indices because of the high Rb content (Rb: 149 ppm, Sr: 186 ppm, Zr: 92 ppm; Figure 3). The high Sr (228–255 ppm) and Zr (325–659 ppm) contents suggest the existence of another weathering horizon between 1316–1380 cm within the L2 loess body. In contrast, based on the grain size composition (Figure 2), the high GSI and high U-ratios, the development of a loess body deposited by intensive wind and dust storms are supposed. The proportion of the finer fractions increases again by the weakening of the assumed storms. Rb reaches a maximum of 151 ppm at 1300 cm, which causes a high Rb/Sr ratio. A paleosol developmental stage can be observed within the diverse S1 paleosol layer, which is characterized by a low concentration of Rb (44–58 ppm). Zr also reaches its minimum in the profile (13 ppm). A definite weathering emerges in the upper part of this paleosol between 904–908 cm, yet below the L1L2/S1 boundary.

Above a weak weathering horizon in the L1L2 loess body between 640–644 cm, a more significant one also can be observed. However, the highest Zr concentration value (1781 ppm) of the profile occurs at 568–572 cm, the weathering horizon appears only above, at the boundary of L1S1/L1L2 with a moderate Zr (98 ppm). Similar results were obtained in the case of L1L1/L1S1 boundary (296–308 cm) with the Zr values of 1023 ppm and then 60 ppm. Despite the weak weathering within the loess body of L1L1, a more intensive sediment accumulation and the intensified wind is assumed based on the GSI and U-ratio. The complete absence of Rb suggests intense weathering in the L1L1/S0 boundary.

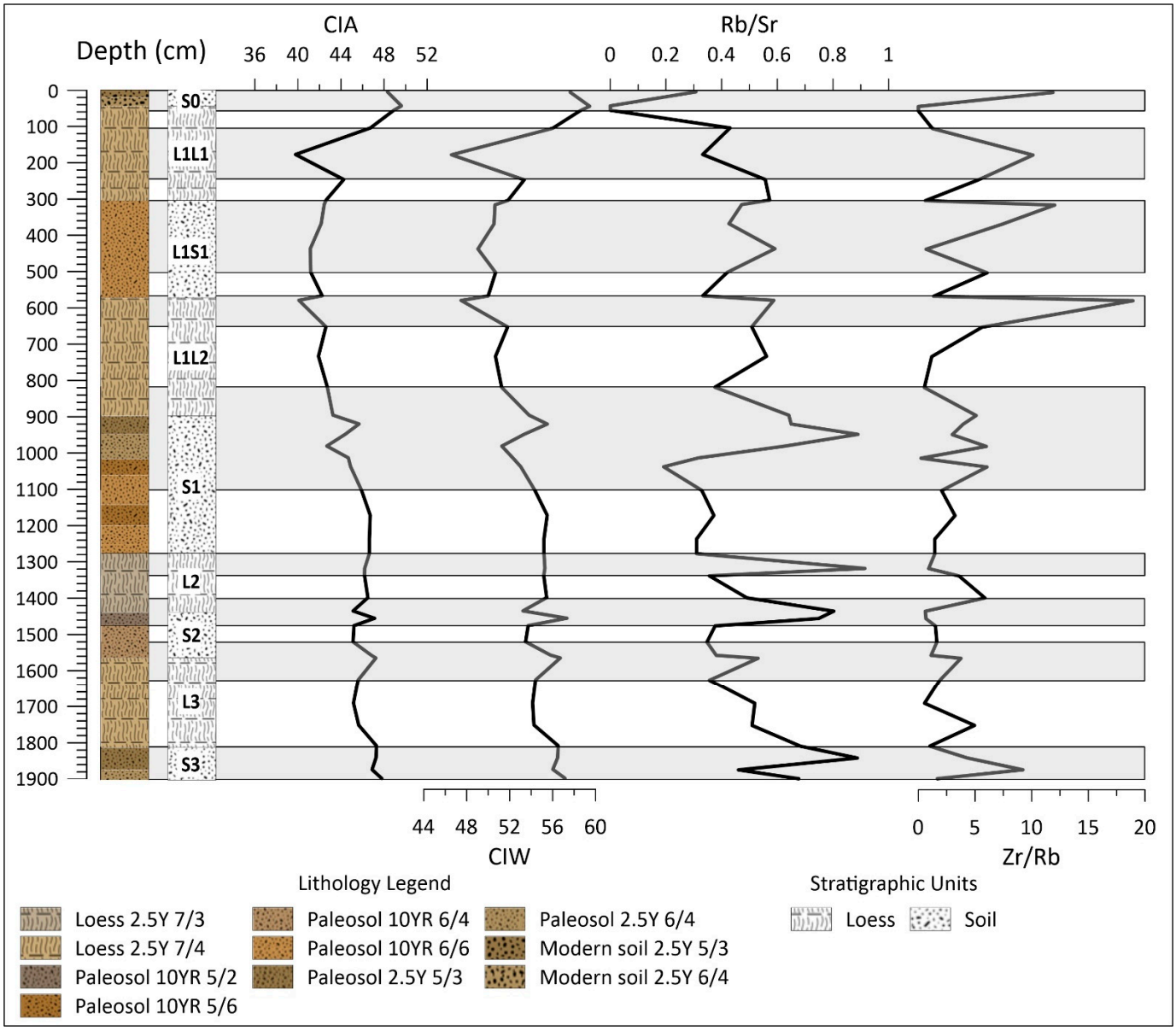

Figure 4. Geochemical indices used to explore weathering in the loess-paleosol sequence.

4. Discussion

Based on the sedimentological results, it can be noted that the complete section is characterized by a high proportion of very fine sand fraction (5–36%). It indicates increased transport energy [20] or the sediments of the surrounding sand dunes and sand sheets. In consistent with previous studies, among all the examined grain composition indices, U-ratio is the one, which indicates cold periods and strong winds with higher values in loess bodies, and warmer periods in paleosols [18,46,48,49]. In addition, the positive peaks of GSI values indicate increased sedimentation rate and frequent powerful dust storms [18,50]. In the case of our profile, two significantly increased and several elongated sections can be observed. The two peaks are detected in the L2 loess body and the L1S1 paleosol. Both parts were characterized by the high proportion of coarser fractions and sharply decreased clay fraction (5%) (Figure 2). Non-significant peaks can be observed in the whole L3 loess body, in the initial parts of the S1 and L1L2, and above the weathering horizon in the L1L1 loess body.

A significant change can be observed in the section at the height of 10 m based on the elemental composition and particle size indices. This can be explained by the complete termination of the supply of dust, rich in sulphide minerals. Under 10 m the values of Mg, P and S major elements are relatively common, even if with small percentages (Mg < 6%, P and S < 0.6%). Trace elements as Zn, Pb, Ni, As are significant below 10 m. Considering the mineral composition of the surrounding areas, the origin of the dust, which presumably consists of sulphide minerals and igneous rocks, could have been the Buda Thermal Karst, the Börzsöny or the Cserhát. Thus, NW as the prevailing wind direction can be assumed. However, further research is necessary for the more precise determination of the exact source area of the sediment.

5. Conclusions

The foothill/hill-situated loess-paleosol profile of Pécel is located in the Gödöllő Hills in the northern part of the Carpathian Basin. The preliminary sedimentological and geochemical investigations have shown that the profile merits conducting further research, as no significant erosion or intensive weathering could be detected. It carries a wealth of data, which can perfectly complement the results of the surrounding profiles investigated so far and could provide data for the study of the climate changes in the Quaternary. The origin of flying dust and the prevailing winds are also can be examined. The change at about 10 m is an evidence of the change of the source area of the accumulated dust. The seemingly opposite results within the L2 loess body may be explained by the further transport of finer fractions (and a sharp decrease in the proportion of clay) because of the increased transport energy and the deposition of larger particles. Similar fluctuations can be seen in the case of GSI in the L1S1 paleosol layer, where the geochemical indices also indicate soil development. Considering the entire profile, weathering horizons occur at the loess-paleosol transition zones. As this is a preliminary examination of the profile, further research will be conducted. Radiocarbon and OSL/IRSL data will be suitable for the determination of the actual age of the profile, age-depth models will be built for the estimation of the volume and the rate of sediment accumulation. Besides, malacological examination of the remaining snail shells of the sediment will provide more accurate information about the paleoecological factors. Finally, magnetic susceptibility results will be applied to correlate the paleosol levels and the MIS stages and that will allow us the correlation of the Pécel profile with similar profiles.

Author Contributions: Conceptualization, L.M., D.M. and P.S.; methodology, L.M., D.M.; software, L.M., D.M. and B.R.; validation, L.M. and D.M.; formal analysis, P.C.; investigation, L.M., D.M., B.R., G.B., P.C. and B.N.; resources, L.M. and P.S.; data curation, L.M.; writing—original draft preparation, L.M.; writing—review and editing, L.M., D.M. and P.C.; visualization, L.M., D.M. and B.R.; supervision, P.S.; project administration, L.M., D.M. and B.R.; funding acquisition, L.M. and P.S. All authors have read and agreed to the published version of the manuscript.

Funding: This research was funded by the Hungarian Government, Ministry of Human Capacities (20391-3/2018/FEKUSTRAT) and the Hungarian National Excellence Program grant NTP-NFTÖ-19-B-0069 (L. Makó).

Data Availability Statement: The data presented in this study are available on request from the corresponding author. The data are not publicly available due to the data will also be used in ongoing research.

Acknowledgments: First of all, we are grateful to Gedeon Rajcsinec for the protection of the area, thus allowing the loess wall to survive and gave us the opportunity for the investigations.

Conflicts of Interest: The authors declare no conflict of interest.

References

1. Kukla, G. Pleistocene land-sea correlations. *Earth-Sci. Rev.* **1977**, *13*, 307–374. [CrossRef]
2. Ding, Z.; Derbyshire, E.; Yang, S.; Sun, J.; Liu, T. Stepwise expansion of desert environment across northern China in the past 3.5 Ma and implications for monsoon evolution. *Earth Planet. Sci. Lett.* **2005**, *237*, 45–55. [CrossRef]
3. Rousseau, D.-D. Statistical analyses of loess molluscs for paleoecological reconstructions. *Quat. Int.* **1990**, *7–8*, 81–89. [CrossRef]
4. Antoine, P.; Rousseau, D.-D.; Zöller, L.; Lang, A.; Munaut, A.-V.; Hatté, C.; Fontugne, M. High-resolution record of the last Interglacial-glacial cycle in the Nussloch loes—Palaeosol sequences, Upper Rhine Area, Germany. *Quat. Int.* **2001**, *76–77*, 211–229. [CrossRef]
5. Zhou, L.P.; Oldfield, F.; Wintle, A.G.; Robinson, S.G.; Wang, J.T. Partly pedogenic origin of magnetic variations in Chinese loess. *Nat. Cell Biol.* **1990**, *346*, 737–739. [CrossRef]
6. Sümegi, P. *Loess and Upper Paleolithic Environment in Hungary: An Introduction to the Environmental History of Hungary*; Aurea: Nagykovácsi, Hungary, 2005; p. 312.
7. Bösken, J.; Sümegi, P.; Zeeden, C.; Klasen, N.; Gulyás, S.; Lehmkuhl, F. Investigating the last glacial Gravettian site 'Ságvár Lyukas Hill' (Hungary) and its paleoenvironmental and geochronological context using a multi-proxy approach. *Palaeogeogr. Palaeoclim. Palaeoecol.* **2018**, *509*, 77–90. [CrossRef]
8. Marković, S.B.; Stevens, T.; Kukla, G.J.; Hambach, U.; Fitzsimmons, K.E.; Gibbard, P.; Buggle, B.; Zech, M.; Guo, Z.; Hao, Q.; et al. Danube loess stratigraphy towards a pan-European loess stratigraphic model. *Earth Sci. Rev.* **2015**, *148*, 228–258. [CrossRef]
9. Song, Y.; Guo, Z.; Marković, S.B.; Hambach, U.; Deng, C.; Chang, L.; Wu, J.; Hao, Q. Magnetic stratigraphy of the Danube loess: A composite Titel-Stari Slankamen loess section over the last one million years in Vojvodina, Serbia. *J. Asian Earth Sci.* **2018**, *155*, 68–80. [CrossRef]
10. Moine, O.; Rousseau, D.-D.; Antoine, P. The impact of Dansgaard–Oeschger cycles on the loessic environment and mal-acofauna of Nussloch (Germany) during the Upper Weichselian. *Quat. Res.* **2008**, *70*, 91–104. [CrossRef]
11. Sümegi, P.; Gulyás, S.; Persaits, G.; GergelyPáll, D.; Molnár, D. The loess-paleosol sequence of Basaharc (Hungary) revisited: Mollusc-based paleoecological results for the Middle and Upper Pleistocene. *Quat. Int.* **2011**, *240*, 181–192. [CrossRef]
12. Sumegi, P.; Nafradi, K.; Molnar, D.; Sávai, S. Results of paleoecological studies in the loess region of Szeged-Öthalom (SE Hungary). *Quat. Int.* **2015**, *372*, 66–78. [CrossRef]
13. Sümegi, P.; Gulyás, S.; Molnár, D.; Almond, P.; Vandenberghe, J.; Zhou, L.; Pál-Molnár, E.; Törőcsik, T.; Hao, Q.; Smalley, I.; et al. New chronology of the best developed loess/paleosol sequence of Hungary capturing the past 1.1 ma: Implications for correlation and proposed pan-Eurasian stratigraphic schemes. *Quat. Sci. Rev.* **2018**, *191*, 144–166. [CrossRef]
14. Sümegi, P.; Molnár, D.; Gulyás, S.; Náfrádi, K.; Sümegi, B.P.; Törőcsik, T.; Persaits, G.; Molnár, M.; Vandenberghe, J.; Zhou, L. High-resolution proxy record of the environmental response to climatic variations during transition MIS3/MIS2 and MIS2 in Central Europe: The loess-paleosol sequence of Katymár brickyard (Hungary). *Quat. Int.* **2019**, *504*, 40–55. [CrossRef]
15. Sümegi, P.; Gulyás, S.; Molnár, D.; Szilágyi, G.; Sümegi, B.P.; Törőcsik, T.; Molnár, M. 14C Dated Chronology of the Thickest and Best Resolved Loess/Paleosol Record of the LGM from SE Hungary Based on Comparing Precision and Accuracy of Age-Depth Models. *Radiocarbon* **2020**, *62*, 403–417. [CrossRef]
16. Molnár, D.; Sümegi, P.; Fekete, I.; Makó, L.; Sümegi, B.P. Radiocarbon dated malacological records of two Late Pleistocene loess-paleosol sequences from SW-Hungary: Paleoecological inferences. *Quat. Int.* **2019**, *504*, 108–117. [CrossRef]
17. Újvári, G.; Kovács, J.; Varga, G.; Raucsik, B.; Marković, S.B. Dust flux estimates for the Last Glacial Period in East Central Europe based on terrestrial records of loess deposits: A review. *Quat. Sci. Rev.* **2010**, *29*, 3157–3166. [CrossRef]
18. Újvári, G.; Kok, J.F.; Varga, G.; Kovács, J. The physics of wind-blown loess: Implications for grain size proxy interpreta-tions in Quaternary paleoclimate studies. *Earth-Sci. Rev.* **2016**, *154*, 247–278. [CrossRef]
19. Bösken, J.; Obreht, I.; Zeeden, C.; Klasen, N.; Hambach, U.; Sümegi, P.; Lehmkuhl, F. High-resolution paleclimatic proxy data from the MIS3/2 transition recorded in northeastern Hungarian loess. *Quat. Int.* **2019**, *502*, 95–107. [CrossRef]
20. Pye, K. The nature, origin and accumulation of loess. *Quat. Sci. Rev.* **1995**, *14*, 653–667. [CrossRef]
21. Rousseau, D.; Antoine, P.; Hatté, C.; Lang, A.; Zöller, L.; Fontugne, M.; Othman, D.; Luck, J.; Moine, O.; Labonne, M.; et al. Abrupt millennial climatic changes from Nussloch (Germany) Upper Weichselian eolian records during the Last Glaciation. *Quat. Sci. Rev.* **2002**, *21*, 1577–1582. [CrossRef]
22. Gallet, S.; Jahn, B.-M.; Lanoë, B.V.V.; Dia, A.; Rossello, E. Loess geochemistry and its implications for particle origin and composition of the upper continental crust. *Earth Planet. Sci. Lett.* **1998**, *156*, 157–172. [CrossRef]
23. Jahn, B.-M.; Gallet, S.; Han, J. Geochemistry of the Xining, Xifeng and Jixian sections, Loess Plateau of China: Eolian dust provenance and paleosol evolution during the last 140 ka. *Chem. Geol.* **2001**, *178*, 71–94. [CrossRef]
24. Hupuczi, J.; Sümegi, P. The late pleistocene paleoenvironment and paleoclimate of the madaras section (South Hungary), based on preliminary records from mollusks. *Open Geosci.* **2010**, *2*, 64–70. [CrossRef]
25. Marosi, S.; Somogy, S. Gödöllői-dombság. In *Magyarország Kistájainak Katasztere II*; Földrajztudományi Kutató Intézet: Budapest, Hungary, 1990; pp. 802–807.
26. Ruszkiczay-Rüdiger, Z.; Fodor, L.; Horváth, E.; Telbisz, T. Folyóvízi, eolikus és neotektonikai hatások szerepe a Gö-döllői-dombság felszínfejlődésében—DEM-alapú morfometriai vizsgálat. *Földrajzi Közlemények* **2007**, *131*, 319–342.
27. Molnár, D.; Makó, L.; Sümegi, P.; Sümegi, B.P.; Törőcsik, T. Revisiting the palaeolithic site at Szeged-Öthalom: Attempt for appoint the palaeolithic horizon. *Studia Quat.* **2019**, *36*, 45–53.

28. Újvári, G.; Varga, A.; Raucsik, B.; Kovács, J. The Paks loess-paleosol sequence: A record of chemical weathering and provenance for the last 800ka in the mid-Carpathian Basin. *Quat. Int.* **2014**, *319*, 22–37. [CrossRef]
29. Újvári, G.; Molnár, M.; Páll-Gergely, B. Charcoal and mollusc shell 14 C-dating of the Dunaszekcső loess record, Hungary. *Quat. Geochronol.* **2016**, *35*, 43–53. [CrossRef]
30. Varga, A.; Újvári, G.; Raucsik, B. Tectonic versus climatic control on the evolution of a loess-paleosol sequence at Bere-mend, Haungary: An integrated approach based on paleoecological, clay mineralogical, and geochemical data. *Quat. Int.* **2011**, *240*, 71–86. [CrossRef]
31. Sümegi, P.; Törőcsik, T.; Náfrádi, K.; Sümegi, B.P.; Majkut, P.; Molnár, D.; Tapody, R. Radiocarbon dated complex pale-oecological and geoarcheological analyses at the Bodrogkeresztúr Henye Gravettian site (NE Hungary). *Archeometriai Műhely* **2016**, *8*, 31–42.
32. Molnár, D.; Makó, L.; Cseh, P.; Sümegi, P.; Fekete, I.; Galovic, L. Middle and Late Pleistocene loess-paleosol archives in East Croatia: Multi-prox palaeoecological studies on Zmajevac and Šarengrad II sequences. *Stud. Quat.* **2021**, *38*, 3–17.
33. Krolopp, E. Malacological analysis of the loess from the archaeological site at Esztergom-Gyurgyalag. *Acta Archeol. Sci. Hung.* **1991**, *43*, 257–259.
34. Sümegi, P. Quatermalacological analysis of Late Pleistocene Loess Sediments of the Great Hungarian Plain. *Malacol. Newsl.* **1995**, *1*, 79–111.
35. Sümegi, P.; Krolopp, E. Quatermalacological analyses for modeling of the Upper Weichselian palaeoenvironmental changes in the Carpathian Basin. *Quat. Int.* **2002**, *91*, 53–63. [CrossRef]
36. Újvári, G.; Molnár, M.; Novothny, Á.; Páll-Gergely, B.; Kovács, J.; Várhegyi, A. AMS 14C and OSL/IRSL dating of the Dunaszekcső loess sequence (Hungary): Chronology for 20 to 150 ka and implications for establishing reliable age–depth models for the last 40 ka. *Quat. Sci. Rev.* **2014**, *106*, 140–154. [CrossRef]
37. Makó, L.; Molnár, D.; Cseh, P.; Sümegi, P. MAR comparisons between different chronometric methods for two profiles in the Bodrogkeresztúr area. *Stud. Quat.* **2021**, *38*, 67–73.
38. Jary, Z. Periglacial markers within the Late Pleistocene loess–palaeosol sequences in Poland and Western Ukraine. *Quat. Int.* **2009**, *198*, 124–135. [CrossRef]
39. Jary, Z.; Ciszek, D. Late Pleistocene loess–palaeosol sequences in Poland and western Ukraine. *Quat. Int.* **2013**, *296*, 37–50. [CrossRef]
40. Wikimedia Commons. Pannonian Basin Geographic Map Blank Cropped. Available online: https://upload.wikimedia.org/wikipedia/commons/2/27/Pannonian_Basin_geographic_map_blank_croped.svg (accessed on 15 May 2021).
41. Gyalog, L.; Síkhegyi, F. *Magyarország földtani térképe, M=1:100,000*; A Magyar Állami Földtani Intézet Kiadványa: Budapest, Hungary, 2005.
42. Google Maps. Available online: https://goo.gl/maps/n5twBG8njBKdCgSR9 (accessed on 15 May 2021).
43. Bokhorst, M.P.; Vandenberghe, J.; Sümegi, P.; Łanczont, M.; Gerasimenko, N.P.; Matviishina, Z.N.; Marković, S.B.; Frechen, M. Atmospheric circulation patterns in central and eastern Europe during Weichselian Pleniglacial inferred from loess grain-size records. *Quat. Int.* **2011**, *234*, 62–74. [CrossRef]
44. Wentworth, C.K. A Scale of grade and class terms for clastic sediments. *J. Geol.* **1922**, *30*, 377–392. [CrossRef]
45. Vandenberghe, J.; Mucher, H.J.; Roebroeks, W.; Gemke, D. Lithostratigraphy and Paleoenvironment of the Pleistocene Deposits at Maastricht-Belvédère, Southern Limburg, the Netherlands in Maastricht-Belvédère: Stratigraphy, Palaeoen-vironment and Archaeology of the Middle and Late Pleistocene Deposits. *Analecta Praehist. Leiden.* **1985**, *18*, 7–18.
46. Vandenberghe, J.; An, Z.S.; Nugteren, G.; Lu, H.; van Huissteden, K. New absolute time scale for Quaternary climate in the Chinese Loess region by grain-size analysis. *Geology* **1997**, *25*, 35–38. [CrossRef]
47. Vandenberghe, J.; Nugteren, G. Rapid climatic changes recorded in loess successions. *Glob. Planet. Chang.* **2001**, *28*, 1–9. [CrossRef]
48. Nugteren, G.; Vandenberghe, J.; van Huissteden, K.; An, Z.S. A Quaternary climate record based on grain size analysis from the Luochuan loess section on the Central Loess Plateau, China. *Glob. Planet. Chang.* **2004**, *41*, 167–183. [CrossRef]
49. Vandenberghe, J. Grazin size of fine-grained windblown sediment: A powerful proxy for process identification. *Earth-Sci. Rev.* **2013**, *121*, 18–30. [CrossRef]
50. Rousseau, D.-D.; Sima, A.; Antoine, P.; Hatté, C.; Lang, A.; Zöller, L. Link between European and North Atlantic abrupt climate changes over the last glaciation. *Geophys. Res. Lett.* **2007**, *34*, 22713. [CrossRef]
51. Dean, W.E. Determination of carbonate and organic matter in calcareous sediments and sedimentary rocks by loss on ig-nition; comparison with other methods. *J. Sediment. Res.* **1974**, *44*, 242–248.
52. Nesbitt, H.; Markovics, G.; Price, R. Chemical processes affecting alkalis and alkaline earths during continental weathering. *Geochim. Cosmochim. Acta* **1980**, *44*, 1659–1666. [CrossRef]
53. Nesbitt, H.W.; Young, G.M. Early Proterozoic climates and plate motions inferred from major element chemistry of lutites. *Nat. Cell Biol.* **1982**, *299*, 715–717. [CrossRef]
54. Liu, C.-Q.; Masuda, A.; Okada, A.; Yabuki, S.; Zhang, J.; Fan, Z.-L. A geochemical study of loess and desert sand in northern China: Implications for continental crust weathering and composition. *Chem. Geol.* **1993**, *106*, 359–374. [CrossRef]
55. Chen, J.; An, Z.; Head, J. Variation of Rb/Sr Ratios in the Loess-Paleosol Sequences of Central China during the Last 130,000 Years and Their Implications for Monsoon Paleoclimatology. *Quat. Res.* **1999**, *51*, 215–219. [CrossRef]
56. Ding, Z.; Sun, J.; Yang, S.; Liu, T. Geochemistry of the Pliocene red clay formation in the Chinese Loess Plateau and implications for its origin, source provenance and paleoclimate change. *Geochim. Cosmochim. Acta* **2001**, *65*, 901–913. [CrossRef]

57. Muhs, D.R.; Bettis, E.A.; Been, J.; McGeehin, J.P. Impact of climate and parent material on chemical weathering in lo-ess-derived soils of the Mississippi River valley. *Soil Sci. Soc. Am. J.* **2001**, *65*, 1761–1777. [CrossRef]
58. Yang, S.; Li, C.; Yang, D.; Li, X. Chemical weathering of the loess deposits in the lower Changjiang Valley, China, and paleoclimatic implications. *Quat. Int.* **2004**, *117*, 27–34. [CrossRef]
59. Schellenberger, A.; Veit, H. Pedostratigraphy and pedological and geochemical characterization of Las Carreras Lo-ess-paleosol sequence, Valle de Tafi, NW-Argentina. *Quat. Sci. Rev.* **2006**, *25*, 811–831. [CrossRef]
60. Tan, H.; Ma, H.; Zhang, X.; Lu, H.; Wang, J. Typical geochemical elements in loess deposits in the Northeastern Tibetan Plateau and its paleoclimatic implications. *Acta Geol. Sin.* **2006**, *80*, 110–117.
61. Jeong, G.Y.; Hillier, S.; Kemp, R.A. Quantitive bulk and single particle mineralogy of a thick Chinese loess-plaeosol section: Implications for loess provenance and weathering. *Quat. Sci. Rev.* **2008**, *27*, 1271–1287. [CrossRef]
62. Jeong, G.Y.; Hillier, S.; Kemp, R.A. Changes in mineralogy of loess–paleosol sections across the Chinese Loess Plateau. *Quat. Res.* **2011**, *75*, 245–255. [CrossRef]
63. Bokhorst, M.P.; Beets, C.J.; Marković, S.B.; Gerasimenko, N.P.; Matviishina, Z.N.; Frenchen, M. Pedo-chemical climate proxies in Late Pleistocene Serbian-Ukrainian loess sequences. *Quat. Int.* **2009**, *198*, 113–123. [CrossRef]
64. Buggle, B.; Glaser, B.; Hambach, U.; Gerasimenko, N.; Marković, S.B. An evaluation of geochemical weathering indices in loess-paleosol studies. *Quat. Int.* **2011**, *240*, 12–21. [CrossRef]
65. Railsback, L.B. An earth scientist's periodic table of the elements and their ions. *Geology* **2003**, *31*, 737–740. [CrossRef]
66. Reeder, S.; Taylor, H.; Shaw, R.A.; Demetriades, A. Introduction to the Chemistry and Geochemistry of the Elements. In *Geochemical Atlas of Europe. Part 2. Interpretation of Geochemical Maps, Additional Tables, Figures, Maps, and Related Publications*; Tarvainen, T., de Vos, M., Eds.; Geological Survey of Finland: Espoo, Finland, 2006; pp. 48–429.
67. Harnois, L. The CIW index: A new chemical index of weathering. *Sediment. Geol.* **1988**, *55*, 319–322. [CrossRef]
68. Chen, J.; Chen, Y.; Liu, L.; Ji, J.; Balsam, W.; Sun, Y.; Lu, H. Zr/Rb ratio in the Chinese loess sequences and its implication for changes in the East Asian winter monsoon strength. *Geochim. Cosmochim. Acta* **2006**, *70*, 1471–1482. [CrossRef]
69. Liang, L.; Sun, Y.; Beets, C.J.; Prins, M.; Wu, F.; Vandenberghe, J. Impacts of grain size sorting and chemical weathering on the geochemistry of Jingyuan loess in the northwestern Chinese Loess Plateau. *J. Asian Earth Sci.* **2013**, *69*, 177–184. [CrossRef]
70. Kukla, G. Loess stratigraphy in central China. *Quat. Sci. Rev.* **1987**, *6*, 191–219. [CrossRef]
71. Kukla, G.; An, Z.S.; Melice, J.L.; Gavin, J.; Xiao, J.L. Magnetic susceptibility record of Chinese Loess. *Earth Environ. Sci. Trans. R. Soc. Edinb.* **1990**, *81*, 263–288. [CrossRef]
72. Cohen, K.; Gibbard, P. Global chronostratigraphical correlation table for the last 2.7 million years, version 2019 QI-500. *Quat. Int.* **2019**, *500*, 20–31. [CrossRef]
73. Marković, S.B.; Bokhorst, M.P.; Vandenberghe, J.; McCoy, W.D.; Oches, E.A.; Hambach, U.; Gaudenyi, T.; Jovanović, M.; Zöller, L.; Stevens, T.; et al. Late Pleistocene loess-paleosol sequences in the Vojvodina region, Serbia. *J. Quat. Sci.* **2008**, *23*, 73–84. [CrossRef]